CEAS Space Journal
https://doi.org/10.1007/s12567-025-00660-5

ORIGINAL PAPER

Designing an electromechanical capture system for in-air capturing of winged RLVs

B. Luyten[1,2] · S. Singh[1] · B. T. C. Zandbergen[2]

Received: 13 January 2025 / Revised: 1 July 2025 / Accepted: 6 August 2025

Abstract
In-air capturing is a promising concept for recovering winged reusable launch vehicles (RLVs) using a towing aircraft (TA), without the need for any propulsion on board the RLV during descent. In this paper, the preliminary electromechanical design of an airborne device is presented, which is central to in-air capturing. The device is an autonomous system, towed by the TA, and docks with a boom attached to the nose of the RLV. A design space exploration and load analysis are performed using a simplified towing model, revealing significantly higher towing loads compared to previous estimates. The design of a probe-drogue docking mechanism is proposed, which uses a set of actuated wedges to lock the RLV boom in place. Actuator and sensor solutions are studied, aiming at a redundant and robust mechanism design. Based on reference commercial-off-the-shelf components, the size, weight, and power footprints of essential avionics are estimated, and a preliminary dimensioning of the required battery system is performed. Finally, a comprehensive, electromechanical computer-aided design model is developed, with which the overall inertial properties of the vehicle are estimated. The position of its centre of gravity is studied, revealing the need for a forward trim mass. Compared to previous design studies, the estimated total mass is increased to 175.44 kg, while the design's overall safety factor grows to 1.51.

Keywords In-air capturing · Aerodynamically controlled capturing device · Electromechanical design · Reusable launch vehicles

List of symbols

α	Angle of attack, deg
γ	Flight path angle, deg
δ	Pitch control deflection, deg
θ	Tether angle, deg
D	Drag, N
e	CoG distance, m
f	Moment reference point distance, m
F	Towing force, N
F_t	Engine thrust, N
g	Gravitational acceleration, m/s^2
H	Altitude, m
L	Lift, N
l_T	Tether length, m
m	Mass, kg
M	Pitching moment, Nm
Ma	Mach number, –
q	CoG contribution, %
x,y	towing position, m

Abbreviations

ACCD	Aerodynamically controlled capturing device
AoA	Angle of attack
CAD	Computer-aided design
CFD	Computational fluid dynamics
COTS	Commercial-off-the-shelf
CoG	Centre of gravity
RLV	Reusable launch vehicle
SWaP	Size, weight, and power
TA	Towing aircraft

1 Introduction

While numerous concepts for launch vehicle reusability have been surfacing all over the space industry, programs such as the Space Transportation System—and various conceptual analyses—have shown that minimizing recovery and

✉ B. Luyten
briek.luyten@ugent.be

[1] Systemanalyse Raumtransport, Deutsches Zentrum für Luftund Raumfahrt, Linzer StraSSe 1, Bremen, Germany

[2] Department of Space Engineering, Delft University of Technology, Kluyverweg 1, Delft, The Netherlands

Published online: 31 August 2025

refurbishment costs is vital to drive down overall launch costs, and increase access to space [1]. Among reusability concepts, the *in-air capturing* approach developed at the German Aerospace Center promises a significant reduction in launch costs, with an expected performance similar to the downrange landing technique practiced by SpaceX [2, 3].

For in-air capturing, shown schematically in Fig. 1, the first stage of a reusable launch vehicle (RLV) is equipped with aerodynamic surfaces. Using these, the RLV decelerates after stage separation, and enters a descending formation flight with a repurposed commercial airliner—the towing aircraft (TA). It is then captured in mid-air by an aerodynamically controlled capturing device (ACCD), which is deployed from the TA like an aerial refueling drogue [4]. After capture, the TA tows the RLV back to the vicinity of a landing site, where it is released. The RLV then executes an autonomous, unpowered descent and landing using its own landing gear on a conventional runway.

Evidently, the ACCD plays a vital role in the in-air capturing procedure. As depicted in Fig. 2, it uses four aerodynamic control surfaces to maneuver relative to the TA, while connected to it via a tether [5]. This allows it to bridge the gap between the TA and RLV while both are flying in formation – which is particularly crucial given the low maneuverability of the RLV, and the limited duration of the available capture window [6, 7]. Reliable relative navigation between the ACCD and RLV requires the use of a combined GNSS/INS/VisNav system [8], while the capture itself is performed by a docking mechanism housed inside the ACCD. Once docked, the ACCD then forms the main structural interface between the RLV and TA, supporting the towing loads generated by the 40-ton RLV during tow-back. Finally, it also handles the release of the RLV from the tethered connection with the TA while near a suitable landing site. This combined functionality of maneuverability, docking and release operations, as well as structural towing interface, makes the ACCD a highly unique aerodynamic vehicle, requiring considerable design efforts.

In previous studies, major key aspects of the in-air capturing technique have been extensively investigated. These include RLV design and return trajectories [2], dimensioning and modeling of the tether [5], and control design for the formation flight between RLV and TA [6]. Especially crucial for successful in-air capturing is the aerodynamic compatibility between the TA and RLV. Hence, detailed studies on the aerodynamic performance of both vehicles have been performed [6, 9]. While the RLV has a lift-to-drag ratio of 6, typical commercial aircraft suitable for the role of TA have lift-to-drag ratios of up to 20. This gap is narrowed by deploying drag-inducing surfaces on the TA during formation flight, such as spoilers and landing gear. In recent years, both full-scale simulations and sub-scale experimental test

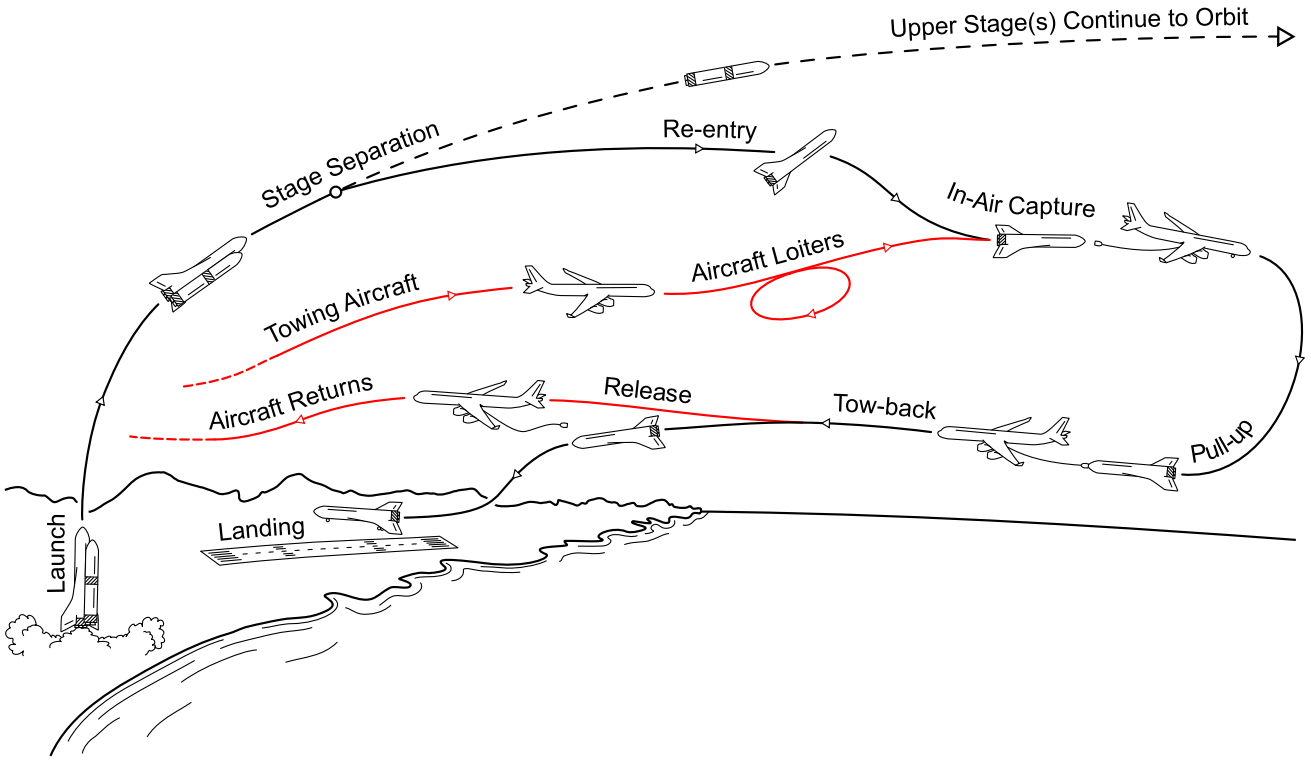

Fig. 1 Schematic overview of the in-air capturing procedure

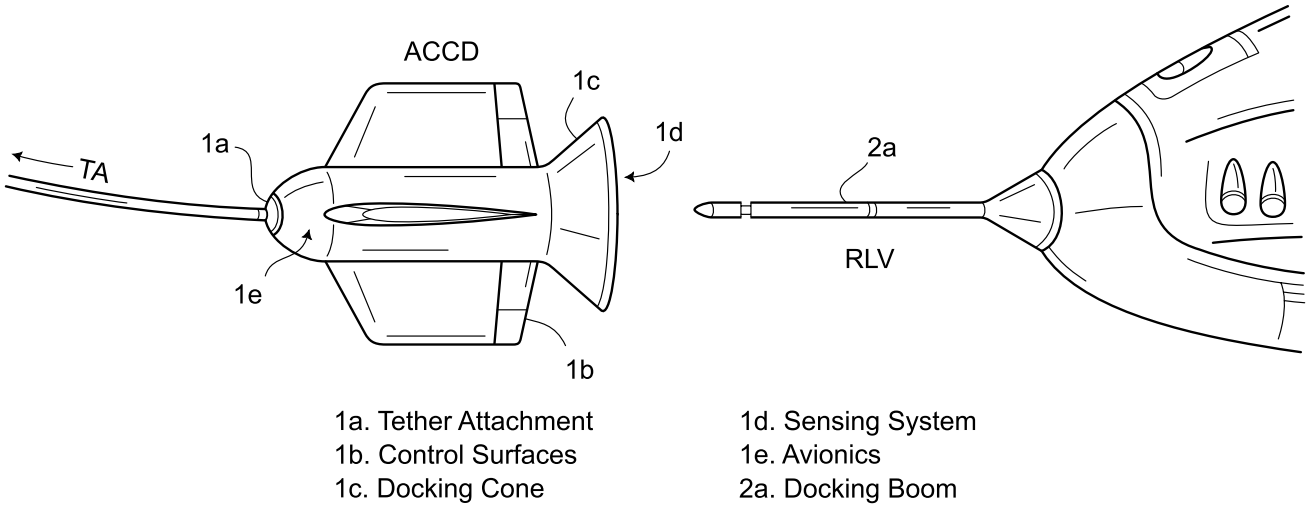

Fig. 2 Schematic view of an aerodynamically controlled capturing device (ACCD), connected to a towing aircraft (TA) and in final approach with a reusable launch vehicle (RLV)

flights have been executed [10–12], demonstrating the potential of this highly innovative reusability concept. As for the ACCD, a preliminary aerodynamic shell has been defined and analyzed, with a total length of 2 m, a 1.5 m wingspan, and NACA0012 aerofoils [13]. Additionally, an initial mechanical study into the ACCD's docking mechanism was performed through computer-aided design (CAD) and finite element analysis [14, 15]. However, this design did not yet cover vital subassemblies such as the tether attachment or wing structure, while major design loads were significantly underestimated. Furthermore, full-scale electronic systems were not yet included, and their impact on the feasibility of the mechanical design was not analyzed. To address these areas of improvement, the current work performs a comprehensive study of the ACCD's electromechanical design space. Using the previously defined aerodynamic shell as a fixed boundary condition, the overall design is reiterated with a better safety factor.

The nature of the ACCD's design is similar to systems used in automated aerial refueling [16] and aerial towing [17], as well as docking mechanisms often employed in space applications [18]. However, significant differences still exist, as aerial refueling applications do not require a structural connection between both vehicles, while in-space docking systems lack the aerodynamic maneuverability required by the ACCD. At the same time, only a limited number of (publicly available) studies have documented the electromechanical design of such systems, so the current study also aims to support design practices in these related fields of application.

First, to characterize the ACCD's inertial design space, and obtain refined estimates for design loads, the behavior of the ACCD as part of an overarching towing system is studied in Sect. 2. This is achieved using a surrogate towing model, which analyses the position of the ACCD relative to the TA, as well as extreme towing forces. Next, a preliminary electromechanical design for the ACCD's docking mechanism is proposed in Sect. 3, based on a probe-drogue methodology. A study is performed regarding the sensors and actuators required to monitor and deploy the mechanism, while its structural strength is studied using finite element analysis. A preliminary estimation for the size, weight, and power (SWaP) footprint of the ACCD's avionics and battery system is then presented in Sect. 4, based on reference commercial-off-the-self (COTS) solutions. Finally, in Sect. 5, a CAD model is developed for the entire electromechanical design, with which the vehicle's inertial properties are estimated.

2 Towing system analysis

To map the ACCD's inertial design space, and analyze extreme towing loads, the overarching towing system is considered. In this study, the *towing system* is defined as all elements connected to the TA: the tether, ACCD, and potentially RLV (during tow-back). Previously, a dynamic, six-degrees-of-freedom model of the towing system was developed in Simulink [5, 10]. However, because of the highly complex nature of this coupled system, simulation is computationally expensive. This impedes an efficient exploration of the available design space, which requires a large number of simulations to quantify the effect of key parameters, such as the ACCD's mass and centre of gravity (CoG). A reduced-complexity surrogate model is thus required, which is able to capture the fundamental behavior of the towing system at a significantly decreased computational

effort. Within the context of the ACCD's design space exploration, the system's steady-state behavior can serve as a first-order approximation to obtain target inertial properties and reference design loads. In reality, any dynamic effects such as tether oscillations, wind gusts, and turbulence will be counteracted as much as possible using the vehicles' control systems. Additionally, highly conservative estimates are used for the steady-state quantities obtained hereafter, to compensate for any missing dynamic contributions.

2.1 Surrogate towing model

To develop the surrogate model, a physics-based method is used rather than a data-based one [19]. This is to avoid a black-box approach and enable insight into the fundamental behavior of the system. A data-based surrogate model would also require a large number of simulations to be performed with the full-scale high-complexity Simulink model – again slowing down the overall design space exploration. Hence, a two-dimensional steady-state model is developed in Python, shown schematically in Fig. 3. Both the ACCD and RLV are represented as finite volumes with a distinct tether attachment, CoG, and moment reference point. Towing loads F_X and F_Y acting at the ACCD's tether attachment are computed using the force and moment equilibria shown in Eq. 1:

$$\begin{cases} F_X = L \cdot \sin\gamma + D \cdot \cos\gamma - m \cdot \ddot{x} \\ F_Y = -L \cdot \cos\gamma + D \cdot \sin\gamma + m \cdot g - m \cdot \ddot{y} \\ M = (L \cdot \cos\alpha + D \cdot \sin\alpha) \cdot (e+f) - \\ \qquad\qquad m \cdot g \cdot e \cdot \cos(\alpha+\gamma) \end{cases} \tag{1}$$

In these equations, γ is the flight path angle, while e and f are the distance of the CoG and moment reference point relative to the ACCD's tether attachment. Lift L, drag D, and pitching moment M are calculated as a function of the ACCD's angle of attack (AoA) α and pitch control deflection δ, using available computational fluid dynamics (CFD) data [9, 20]. During tow-back, when the RLV is attached to the ACCD, the latter's aerodynamic influence is neglected [21]. $g = 9.81\ m/s^2$ is the gravitational acceleration, while m is the mass of the ACCD (and RLV during tow-back). $m \cdot \ddot{x}$ and $m \cdot \ddot{y}$ represent d'Alembert contributions to the towing loads resulting from excess thrust applied by the TA [22]. They are calculated with Eq. 2, where primed quantities refer to the TA. m_T is the tether's mass, while F_t is the TA's thrust, based on propulsion data obtained with the GasTurb tool [23]. In all equations, the 1976 US Standard Atmosphere is used to model the altitude-dependence of air density and temperature [24].

$$\begin{cases} \ddot{x} = \dfrac{-F_t \cdot \cos(\alpha'+\gamma) + (L+L') \cdot \sin\gamma}{m+m'+m_T} + \\ \qquad\qquad \dfrac{(D+D') \cdot \cos\gamma}{m+m'+m_T} \\ \ddot{y} = \dfrac{F_t \cdot \sin(\alpha'+\gamma) + (L+L') \cdot \cos\gamma}{m+m'+m_T} - \\ \qquad\qquad \dfrac{(D+D') \cdot \sin\gamma}{m+m'+m_T} - g \end{cases} \tag{2}$$

Finally, the two-dimensional towing position (x, y) of the ACCD is computed relative to the TA, expressed in a local-vertical, local-horizontal reference frame, centered around the TA's tether attachment. For this, the tether is modeled as a catenary, negligibly influenced by lift and drag [5]. Under this assumption, the ACCD's towing position is given by Eqs. 3 and 4, where l_T is the length of the tether:

$$\begin{cases} x = \dfrac{\operatorname{arsinh}(\tan\theta_1) - \operatorname{arsinh}(\tan\theta_2)}{\tan\theta_1 - \tan\theta_2} \cdot l_T \\ y = \dfrac{\sec\theta_1 - \sec\theta_2}{\tan\theta_1 - \tan\theta_2} \cdot l_T \end{cases} \tag{3}$$

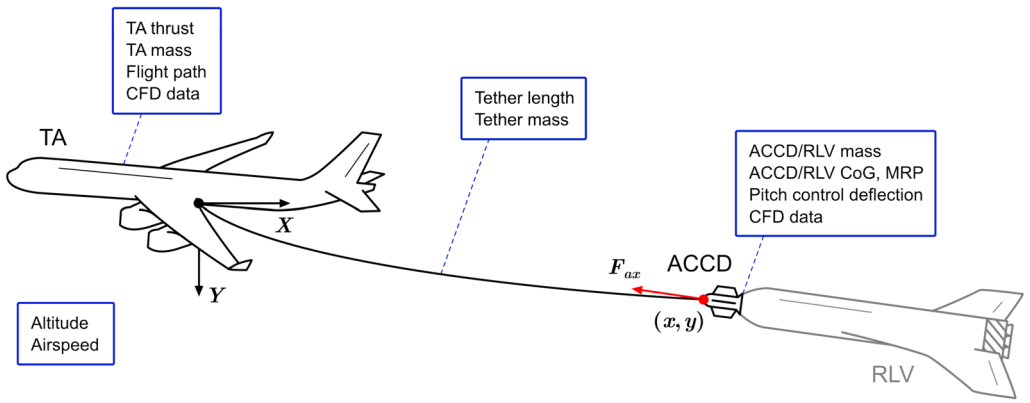

Fig. 3 Schematic setup of the towing model, with main inputs (blue) and outputs (red)

$$\text{where} \begin{cases} \theta_1 = \arctan(F_Y/F_X) \\ \theta_2 = \arctan((F_Y + m_T \cdot g)/F_X) \end{cases} \quad (4)$$

Fixed nominal values for relevant parameters are defined in Table 1, while the main variable parameters are the ACCD's mass m, axial CoG position e, and pitch control deflection δ, as well as the TA's engine thrust, altitude and air speed.

Figure 4 shows part of the model verification efforts, where results from the surrogate towing model are compared to the transient simulation obtained with the Simulink model. This comparison shows that steady-state results differ less than 5% between both models, while the newly proposed model arrives at these conditions in around 0.1% of the computational time—49 ms compared to 44 s required by the Simulink model. Since a 1.5 safety factor is applied to towing loads obtained from this model, the <5% discrepancy between the surrogate model and the Simulink model is deemed acceptable for the purpose of this study. For the ACCD's inertial design space exploration, a similarly conservative approach is used.

With an efficient surrogate towing model established, capable of performing multiple simulations in less than a second, the ACCD's inertial design space can now be explored. This is done by studying the effect of the ACCD's mass, CoG location, and pitch control deflection on its towing position. Additionally, the model can be used to estimate extreme towing loads, by investigating the influence of the TA's thrust, flight altitude, and airspeed on the towing forces.

2.2 Inertial design space

As the ACCD is towed behind the TA, it is at risk of being affected by the latter's wake—which significantly constrains the ACCD's available inertial design space. Because of its disturbing nature, the ACCD should avoid this turbulent region of airflow at all times [7]. Hence, a no-go zone is defined behind the TA, subtending an angle of 7.5° below its flight path—which is based on a CFD characterization of the wake [9]. By staying clear of this no-go zone, the ACCD can avoid the most disturbing region of the wake, for TA AoAs of up to 10° [22]. At the same time, to intercept the RLV, the

Table 1 Nominal towing model inputs during formation flight and tow-back

Variable	Nominal value
l_T	250 m
m_T	85.3 kg
γ (formation flight)	−6.5°
γ (tow-back)	0°
m (RLV)	80 Mg
e (RLV)	41 m

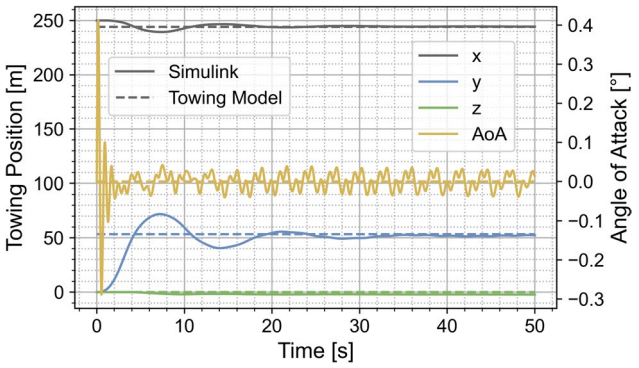

Fig. 4 Comparison of steady-state ACCD position and angle of attack (AoA) between surrogate towing model and Simulink model

ACCD requires a sufficiently large operational range *below* the wake—allowing a vertical translation of at least ±30 m relative to its neutral position [22]. Taking into account the 10° deflection limit of the ACCD's control surfaces [25], the towing model reveals that such an operational range requires a pitch control trim of 7°, with a control surplus of 3° in both directions. Within this context, trim refers to the control deflection required for aerodynamic stability at the desired operational point (i.e., towing position and flight conditions). As shown in Fig. 5, this, in turn, means that the upper towing position should correspond to a 4° control deflection or less.

To translate this upper control deflection requirement into the inertial design space of the ACCD, the design map shown in Fig. 6 can be used—obtained with the towing model. For given inertial properties (mass and CoG), it indicates the minimal control deflection required to stay below the wake no-go zone. The mainly horizontal nature of the iso-deflection curves shows that the ACCD's towing position is largely insensitive to its total mass—especially above 100 kg. On the other hand, the vehicle's CoG position has a significantly more pronounced effect. The design map also shows that configurations with a small mass,

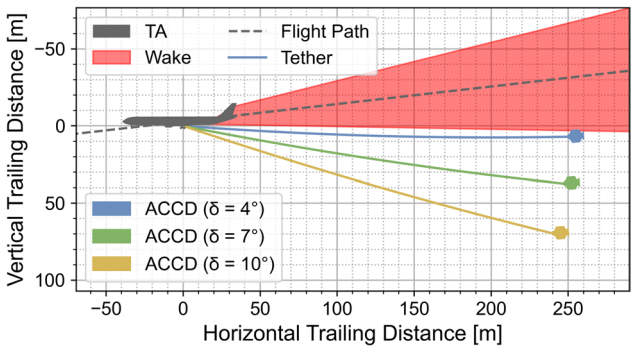

Fig. 5 Required operational range (yellow-blue) of the ACCD, relative to its trimmed towing position (green)

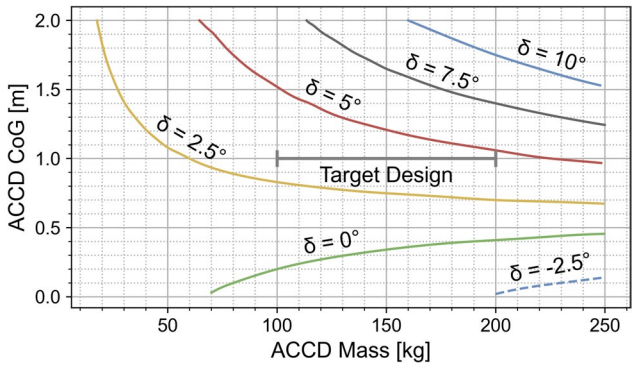

Fig. 6 Inertial ACCD design map: minimal pitch control deflection required to stay below the TA's wake

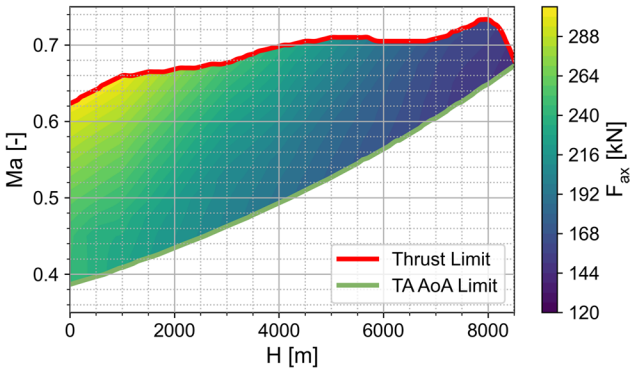

Fig. 7 Influence of tow-back flight altitude H and Mach number Ma on the magnitude of axial towing loads F_{ax}, under full-thrust conditions

and front-located CoG position (i.e., lower left corner of the map) require less control deflection to stay below the wake, resulting in a larger control surplus and operational range. Hence, all configurations *below* the $\delta = 4°$ curve can offer the control surplus required for a ± 30 m operational range. As previous studies estimated the ACCD's mass between 100 and 200 kg [10, 13], this can further be simplified by requiring that the vehicle's CoG be positioned no further than 1 m behind its nose. In previous studies, a target position of 0.6 m was proposed based on a more rudimentary analysis [13].

2.3 Preliminary load analysis

To obtain structural requirements for the primary load-bearing elements inside the ACCD, an estimation for extreme operational forces is required. These occur during tow-back, when the RLV exerts significant towing loads on the ACCD [22]. The magnitude is strongly dependent on the environmental conditions of the tow-back flight, governed by the flight altitude H and Mach number Ma. Figure 7 shows a corresponding sensitivity study, applying full TA engine throttle at all times—with thrust levels also depending on the flight regime [26]. The range of realistic tow-back conditions is limited by the TA's engine performance, as well as a 5° 5° AoA limit [22].

Based on this study, extreme tow-back conditions shown in Eq. 5 are defined. While 1000 m corresponds to the expected RLV release altitude, this operational point is a substantial overestimation of realistic tow-back conditions, which will occur at a higher altitude, and lower velocity [22]. The overestimation serves as a safety margin for the additional effect of dynamic loads, which are not captured by the towing model. Additionally, a 1.5 yield safety factor is applied in subsequent structural analyses [27].

$$\begin{cases} H = 1000\,\text{m} \\ Ma = 0.65 \end{cases} \tag{5}$$

To address the influence of the RLV's towed position on the towing loads, two edge cases are further defined—where the RLV is positioned 1.5° and 10° below the TA's flight path. The former limit is imposed to prevent the tether from interfering with the TA's fuselage, while the latter is an operational boundary condition to limit loads on the RLV [22]. Additionally, a 5% increase relative to the RLV's nominal mass is considered as an additional margin. Under these conditions, the axial towing loads corresponding to the upper and lower RLV positions are 293.2 kN and 299.6 kN, respectively. Based on this analysis, a 300 kN design load is proposed, reflecting a 72% increase compared to previous estimates [28]. The axial loads on the ACCD are driven by drag generated by the RLV, while the RLV's weight is almost entirely counteracted by its own lift-generating surfaces.

3 Docking mechanism design

Based on the foregoing design space exploration, a preliminary design for the ACCD's electromechanical interior is proposed. Its general structure is shown schematically in Fig. 8 and builds upon subassemblies identified during previous studies [14, 15]. Because the docking system comprises the functional core of the ACCD, while its aft location has a potentially unfavorable effect on the overall CoG, its design requires special attention.

3.1 Functional principle

The proposed design of the docking mechanism relies on a probe-drogue principle, where a boom attached to the nose of the RLV (the probe) is inserted into a guiding cone at the ACCD's aft (the drogue) [18]. The conical surfaces of the

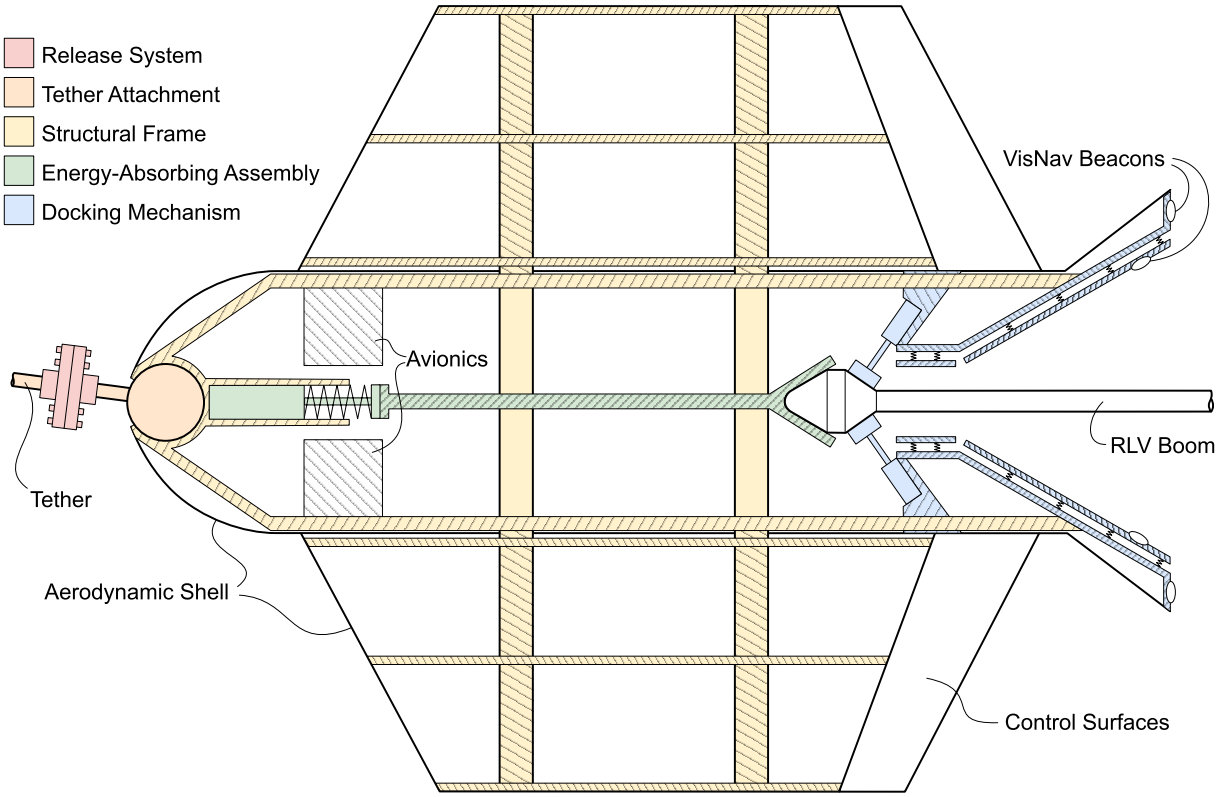

Fig. 8 Schematic overview of the main subassemblies inside the ACCD

boom and guiding cone aid in reducing initial misalignments between the RLV and ACCD, guiding the tip of the boom towards the throat of the guiding cone. Additionally, spring elements in the guiding cone absorb shocks associated with the initial contact between the ACCD and RLV [14]. This design is favored over alternative, androgynous systems, to reduce complexity and accommodate all roll orientations between both vehicles when docking [17, 29].

At the throat of the guiding cone, the RLV boom enters a *locking* mechanism, shown schematically in Fig. 9. It uses a set of four actuated wedges that prevent the RLV boom from exiting the mechanism when deployed. The wedges are actuated in a plane perpendicular to the axial towing direction, so that the actuators themselves remain unloaded. The aft conical surface of the RLV boom provides a structural interface for the wedges, which transfer towing loads onto the ACCD's main structural frame.

Additionally, the tip of the RLV boom interfaces with an energy-absorbing assembly, which uses an industrial shock absorber to accommodate the energy difference between the ACCD and RLV when docking [14]. Because of the spring element inside the industrial shock absorber, a compressive force is exerted on the boom once the compressive energy-absorbing stroke has been completed. In addition to the tensile towing loads on the RLV boom, this clamps the locking mechanism together and helps maintain a locked state throughout tow-back.

3.2 Structural analysis

To verify the structural integrity of the proposed locking mechanism, a preliminary CAD model is developed with CATIA. A finite element analysis is then performed using the Ansys *Static Structural* package, where the (300 kN) axial towing design load is applied to the RLV boom, while rigid supports are added at the mechanism's interface to the ACCD's structural frame. The contact surfaces between the RLV boom and locking wedges, as well as between the locking wedges and the structural ring, are modeled as rough interfaces. For all elements (RLV boom, locking wedges, and structural ring) an Al2024-T6 aluminum alloy is used, with key properties listed in Table 2 [30, 31]. Equivalent von Mises stress under these conditions is then analyzed, as shown in Fig. 10. The resulting peak stress of 223 MPa in the locking mechanism, and 189 MPa in the RLV boom, correspond to a yield safety factor of 1.55 and 1.83, respectively. Additionally, deformations remain below 0.61 mm, while the mechanism is designed to accommodate deformations of up to 1 mm without compromising the docking functionality [22].

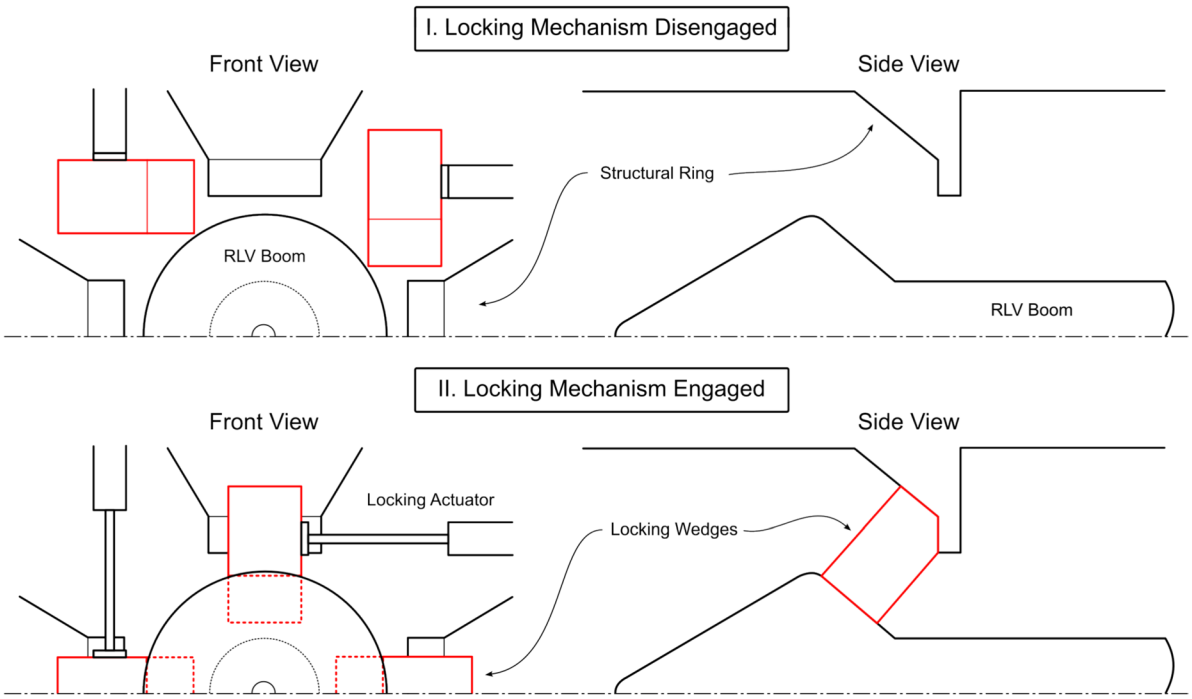

Fig. 9 Functional principle of the proposed locking mechanism design

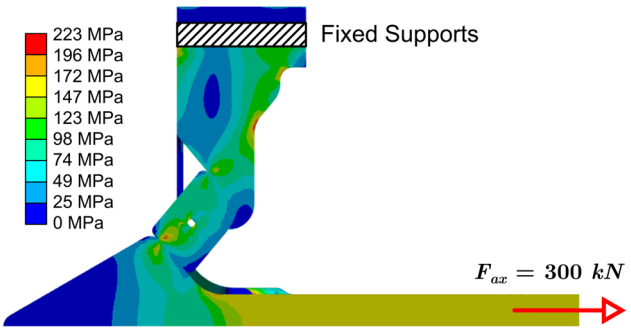

Fig. 10 Equivalent von Mises stress in locking mechanism design under a 300 kN towing load (side view cross-section)

Table 2 Key mechanical properties of Al2024-T6 alloy [30, 31]

Property	Value
Yield strength	345 MPa
Modulus of elasticity	72.4 GPa
Poisson's ratio	0.3
Density	2700 kg/m^3

3.3 Locking actuators

To engage the locking mechanism, a set of four linear actuators is used. Based on the geometry of the proposed mechanism, they require a stroke of at least 80 mm, while having a compressed length of less than 200 mm. Furthermore, full extension should be achieved in less than 0.5 s to ensure rapid and effective deployment of the mechanism [22]. Additionally, if the mechanism is to be released at the end of the tow-back flight, the actuators need to supply sufficient force to retract the wedges from between the RLV boom and ACCD frame. However, the (300 kN) axial towing load exerted on the boom results in significant frictional forces that need to be overcome during the release stroke. Even when considering lubricated aluminum interfaces, the required release force exceeds 10 kN, which is unfeasible given the ACCD's available SWaP budget.

Hence, a separate release system is proposed, shown in Fig. 11. It uses two flanges, each mounted to one end of the tether, and joined with a set of pyrotechnic fasteners. When the charge inside these fasteners is initiated, the flanges are separated, and the tether connection between the RLV and TA is released. The loose tether end is reeled in by the TA, while the ACCD remains attached to the nose of the RLV during its landing—after which it can be disengaged on the ground. The inclusion of this dedicated release system marks an important milestone in the development of the ACCD, as previous studies implicitly assumed the feasibility of a combined docking-and-release mechanism.

Because of the separate release system, load requirements for the locking actuators are drastically reduced. In order to deploy a 286 g wedge within 0.5 s, they only need to supply an extension force of 0.55 N. Taking into account the

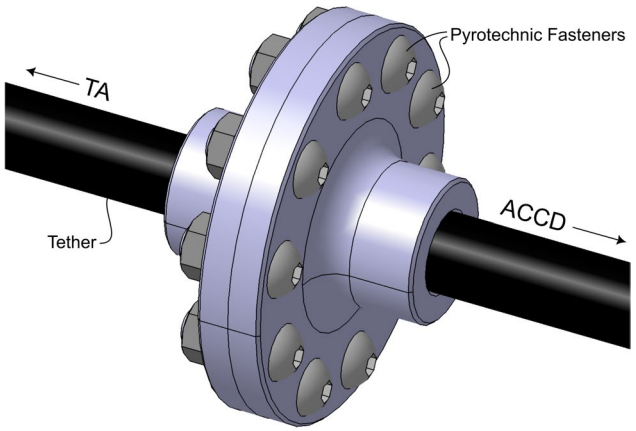

Fig. 11 Schematic of the proposed pyrotechnic release system design concept

geometrical constraints mentioned earlier, COTS solutions can be found that meet all requirements. As a reference, the LM1247-100-11 linear DC actuator developed by Faulhaber is used to estimate the SWaP footprint of these actuators [32].

3.4 Docking sensors

To monitor the RLV docking sequence, and activate the locking mechanism, the proposed design includes three sets of sensors, shown in Fig. 12. Four acoustic distance measuring sensors (e.g., Baumer U300.D50-DPMJ.72N [33]) are located at the entrance to the locking mechanism and detect when the RLV boom is inserted. Arranged in a circular pattern, their different distance measurements can be combined to estimate the local boom thickness. Given the diverging-converging geometry of the RLV boom's tip, this can in turn be converted into an estimation for the axial position of the RLV with respect to the ACCD—priming the activation of the locking mechanism.

Additionally, the compression of the energy-absorbing assembly triggers the activation of a set of grooved photoelectric sensors (e.g., Omron E3Z-G62 [34]). In turn, they command the deployment of the locking mechanism. The axial position of these sensors can be modified to configure the exact timing of the trigger pulse, so that the locking mechanism is only deployed when the RLV boom is sufficiently inserted into the ACCD. Furthermore, the signal from the photoelectric sensors is fused with the boom measurements obtained by the acoustic sensors, to reduce the risk of false positives. By doing so, an undesired or premature deployment of the locking mechanism can be prevented in case of faulty sensor readouts. Finally, the proposed COTS locking actuators include analog Hall-effect sensors [32], which monitor the deployment of the locking mechanism.

As the docking functionality of the ACCD is crucial for in-air capturing to be successful, proper risk analysis and mitigation are essential. Table 3 presents an overview of the most critical failure modes during this operational phase, and the corresponding mitigation strategies implemented in

Table 3 Overview of critical docking failure modes and corresponding risk mitigation strategies

Failure mode	Mitigation strategy
High relative velocity between ACCD and RLV during docking	Integrated shock absorber can accommodate relative velocities up to 8 m/s; full-scale simulations show velocity below 3.5 m/s [26]
Acoustic sensor fails	Sensor redundancy (4×)
Acoustic sensors incorrectly detect RLV boom	Two-step arm/fire mechanism: locking actuators only activate when photoelectric sensors are also triggered
Photoelectric sensor fails	Sensor redundancy (2×)
Locking mechanism jams	Low-complexity mechanism design; appropriate lubrication
Improper docking jeopardizes safety of the TA	Release mechanism doubles as emergency release

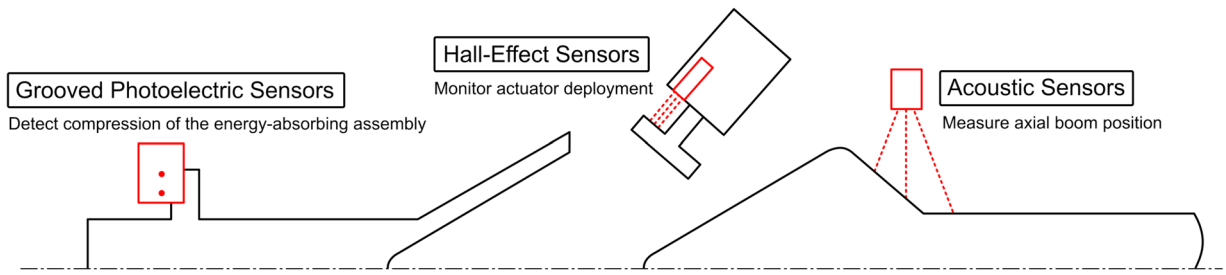

Fig. 12 Overview of the proposed sensor solution for monitoring the docking mechanism

the proposed ACCD design. Notably, the fusion of three distinct types of docking sensors, and their corresponding data diversity, significantly increase the robustness of the overall system. Furthermore, the proposed sensor redundancy eliminates single points of failure, greatly reducing the likelihood of sensor-related failure modes.

4 Avionics and battery system

The overall SWaP footprint of the ACCD's avionics and battery system is estimated based on reference COTS solutions, such as the locking actuators identified in Sect. 3.3, or the docking sensors described in Sect. 3.4. Apart from these systems, the ACCD also requires control actuators, for which an electromechanical design is proposed [22]. Additionally, relative navigation between the ACCD and RLV during formation flight is enabled by a combined GNSS/INS/VisNav system [8]. For this, a set of twelve 1.5 W infrared beacons are mounted along the ACCD's guiding cone, while a separate GNSS module is incorporated in the design. INS data is obtained using gyroscopes and accelerometers integrated into the vehicle's on-board computer [22]. Finally, a radio-frequency communication module is included, to allow the transmission of telemetry to the TA, as well as the communication of relative navigation data with the RLV. The corresponding estimated mass and power footprints of all avionics systems are listed in Table 4. Here, peak power consumption is considered, in order to generate conservative battery requirements. This compensates for any inaccuracies caused by the simplified dimensioning of the power system hereafter.

Preliminary dimensioning of the battery system is performed by defining three operational modes for the ACCD's electronics: *homing*, *towing*, and *release*. *Homing* mode starts with the deployment of the ACCD from the TA, and ends with the successful capture of the RLV. It is estimated to last no longer than 10 min while requiring all avionics to be active. The ACCD is in *towing* mode as long as the RLV is connected to the TA. Based on a reference tow-back flight, from 4° 59' 10" N, 46° 5' 6" W to the vicinity of the Guiana Space Centre [26], the maximum duration of this mode is estimated at 2 h 15 m—assuming a ground speed of at least Mach 0.3 [22]. Finally, the *release* mode starts just before the RLV is released, and ends with its touchdown. Its duration is estimated at 10 min.

When the ACCD is in *towing* or *release* mode, not all electronic systems need to be active. As shown in Table 5, some systems are certainly required during these modes (indicated with a '+'), while other systems still present some uncertainty in terms of their power footprint (indicated with a '−'). Analyzing the combined battery requirements for the ACCD during each operational mode, this uncertainty is translated into lower and upper power estimates.

Cumulative energy requirements for the ACCD are then obtained by combining the estimated power footprints and nominal durations of each operational mode. These result in an energy requirement in the range of 240–625 Wh. Based on this analysis, a preliminary battery system is proposed, consisting of four 175 Wh lithium-ion batteries, which provide an energy margin of 12% compared to the upper power estimates, and 192% compared to the lower ones. The mass and volume of this system are estimated based on typical 175 Wh/kg and 450 Wh/l power densities for lithium-ion technology [35, 36]. It results in a total battery mass of 4 kg, with individual battery dimensions of 100x70x60 mm^3. Given that lithium-ion batteries can achieve power densities well above 250 W/kg [37], the peak power requirement of 970 W during *homing* mode poses no problem.

The proposed mounting system for the batteries is shown in Fig. 13, which interfaces with the structural frame of the ACCD. This polyvalent and modular system allows for a straightforward addition or removal of battery units, while also being capable of accommodating other avionics, such as the on-board computer. Furthermore, the axial position

Table 4 Estimated mass and (peak) power footprints of essential avionics systems

Subsystem	Mass [kg]	Power [W]
On-board computer	0.1	18
Communication module	0.1	6.6
GNSS module	0.1	1.5
VisNav beacons	0.6	18
Control actuators	3.4	816
Locking actuators	0.3	103.3
Acoustic sensors	0.1	4.2
Photoelectric sensors	0.1	1.9

Table 5 Active (+) and potentially active (−) avionics during the ACCD's operational modes, and corresponding power consumption estimates

Subsystem	Homing	Towing	Release
On-board computer	+	+	+
Communication module	+	+	+
GNSS module	+	+	+
VisNav beacons	+		
Control actuators	+		−
Locking actuators	+	−	−
Acoustic sensors	+	+	+
Photoelectric sensors	+	+	+
Total power (lower) [W]	969.5	32.2	32.2
Total power (upper) [W]	969.5	135.5	951.5

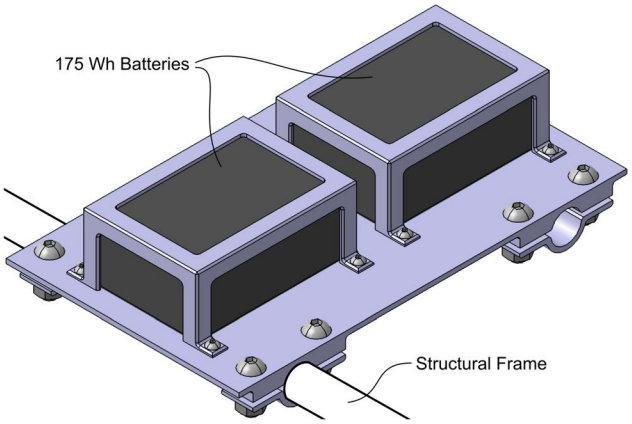

Fig. 13 Computer-aided design (CAD) model of the proposed battery mounting system

of these mounts inside the ACCD can be adjusted, to aid in obtaining a desired CoG position.

5 Design overview

By integrating the battery system and avionics into the structural design of the ACCD, a comprehensive electromechanical CAD model is obtained in CATIA. It includes a preliminary estimation of fasteners, while considering manufacturability and assembly procedures. A cutaway view of the final model is shown in Fig. 14.

Most structural elements in this model are represented by a 2700 kg/m^3 aluminum alloy—either Al2024-T6 or Al6061-T3 [31]. Additionally, a 7800 kg/m^3 density is assumed for the included steel fasteners, as well as for the spring elements inside the guiding cone. For COTS solutions, such as the industrial shock absorber, available technical data is used to model the component as a homogeneous volume with the same total mass [38].

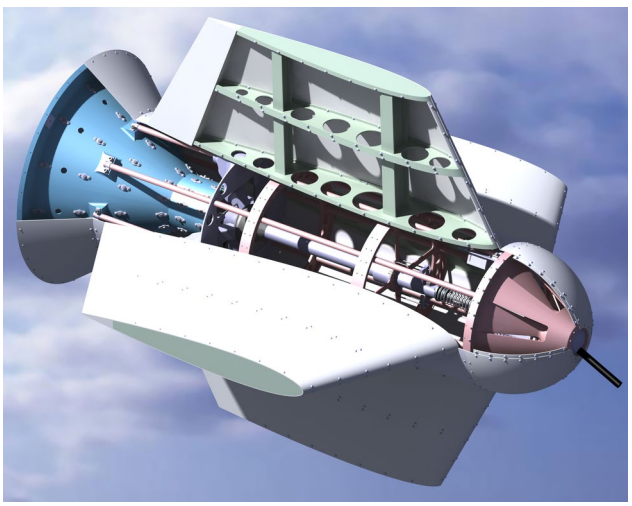

Fig. 14 Cutaway view of the integrated CAD model of the proposed ACCD design

5.1 Mass and stress breakdown

The CAD model is then used to estimate the ACCD's total mass, which is broken down per subassembly in Table 6. The total functional vehicle mass amounts to 159.14 kg, of which the wings constitute 43%. Additionally, the body shell and guiding cone contribute significantly to the total vehicle mass, with the latter being over-dimensioned to offer a safety margin for the uncertainty concerning its structural strength.

The breakdown also includes the overall yield safety factor of each analyzed assembly, resulting in a total safety factor of 1.51. The tether attachment, tether joint, load-bearing frame and locking mechanism were analyzed using the 300 kN axial design load derived in Sect. 2. A uniform 15 kN aerodynamic load was applied to the wing structures, corresponding to the extreme scenario of a 90° AoA in a 200 m/s airflow, at an altitude of 1000 m. Finally, a 30 kN compressive load was used to model the docking impact on the energy-absorbing assembly, based on the industrial shock absorber's technical data [38]. No structural analysis was performed on the guiding cone, body shell, avionics, or battery system.

5.2 Centre of gravity

Combining the estimated mass of each subassembly with their axial position inside the ACCD, the location of the vehicle's overall CoG is further estimated. A uniform density is assumed for individual components, while their CoG positions are calculated with CATIA. The overall CoG is then computed as a weighted average of the individual CoG contributions. A breakdown of these contributions q

Table 6 Mass and stress breakdown of the proposed ACCD design

Assembly	Mass [kg]	SF [–]
Tether attachment	5.944	1.55
Tether joint	1.371	1.81
Load-bearing frame	15.696	1.51
Wing structures	68.396	1.57
Energy-absorbing assembly	8.463	1.56
Locking mechanism	9.827	1.55
Guiding cone	21.789	N/A
Body shell	21.872	N/A
Avionics and batteries	5.783	N/A
Trim mass	16.300	N/A
Total	175.440	1.51

Table 7 Centre of gravity (CoG) breakdown of the proposed ACCD design

Assembly	CoG [m]	q [%]
Tether attachment	0.17	0.6
Tether joint	0.05	0.0
Load-bearing frame	0.93	8.3
Wing structures	1.02	39.8
Energy-absorbing assembly	0.48	2.3
Locking mechanism	1.40	7.8
Guiding cone	1.82	22.6
Body shell	1.11	13.8
Avionics and batteries	0.56	1.8
Trim mass	0.30	2.8
Total	1.00	100.0

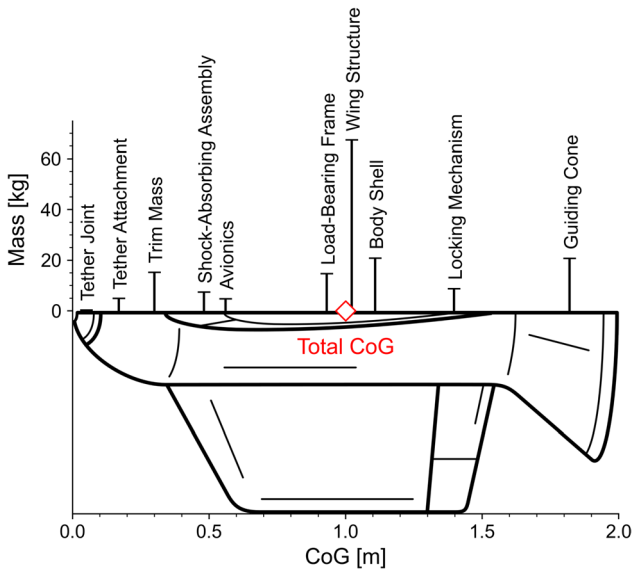

Fig. 15 Visualization of the masses and CoGs of the different subassemblies included in the proposed ACCD design

is shown in Table 7—grouped per subassembly. They are calculated with Eq. 6, where e_i and m_i are the axial CoG distance and mass of the individual subassembly, while m and e are the total mass and axial CoG distance of the overall vehicle—where CoG distances are measured from the ACCD's nose. Figure 15 further visualizes the individual CoGs and mass contributions of the different subassemblies in the ACCD design.

$$q = \frac{e_i \cdot m_i}{e \cdot m} \tag{6}$$

This breakdown reveals that the ACCD's wings and guiding cone are the main contributors to its overall CoG. The former is driven by the wing's significant structural mass, while the latter is a result of the aft location of the guiding cone—in combination with its substantial mass. Although the vehicle's batteries, energy-absorbing assembly, and tether attachment are positioned as much towards the ACCD's nose as possible, they are not capable of fully compensating for this effect. As a result, the total functional mass of the ACCD has a CoG located 1.08 m behind its nose. Because this conflicts with the maneuverability requirement defined in Sect. 2, an additional trim mass is needed. It can realistically be positioned as close as 0.3 m behind the ACCD's nose, and must be at least 16.3 kg for the vehicle's overall CoG position to be within the allowable range. A similar need for a trim mass was also identified in previous studies [13].

5.3 Comparison with previous studies

Comparing the proposed ACCD design with the most recent design iteration performed by Heide, Atanassov, and Stappert [13–15], this study reveals a number of essential changes. The previous design had a total functional mass of 123.9 kg, and a CoG positioned 1.04 m behind the vehicle's nose, requiring an additional 7.6 kg trim mass to attain a 1 m CoG position [22]. Looking at the current study, the ACCD's functional mass has increased by 28.4%. This can be understood by the fact that all design loads have significantly increased compared to previous studies—with as much as 72%. Additionally, the design's safety factor has significantly grown from 1.19 to 1.51 [22].

Because the new design has a higher functional mass, with a further aft-located CoG, a larger trim mass is required. As a result, the total mass estimate for the ACCD has increased by 33% compared to the reference design by Heide et al. These updated mass estimates are important inputs for future studies, in order to represent the behavior of the ACCD more accurately during formation flight, towback, and release.

6 Conclusion

To radically increase access to space, the in-air capturing technique proposes to recover the first stage of a reusable launch vehicle (RLV) by capturing it in mid-air with a towing aircraft (TA), and towing it back to the vicinity of a landing site, where it is released. Central to this technique is the so-called aerodynamically controlled capturing device (ACCD), which is deployed from the TA using a tether, and is responsible for docking, towing, and releasing the RLV. In this paper, a comprehensive design space exploration for such an ACCD was performed, with the aim of addressing knowledge gaps concerning its electromechanical design.

For this, a two-dimensional steady-state towing model was developed as a surrogate for a more complex,

time-consuming alternative. The model captures the behavior of the ACCD while being towed by the TA, and potentially docked to the RLV. Studies performed with the model concerning the operational range of the ACCD showed that its centre of gravity (CoG) has a substantial impact on its towed position relative to the TA. To avoid the disturbing wake zone behind the TA, while maintaining sufficient room for maneuvering and control surplus, the ACCD's CoG should be located no more than 1 m behind its nose. Additionally, sensitivity studies during the tow-back phase show that peak towing loads can be significantly higher than previous estimates assumed. Based on these studies, a 300 kN axial design load is defined—representing a 72% increase. While this value is a deliberate overestimation of steady-state conditions to account for omitted dynamic effects, future studies should verify how representative this design load is for actual peak dynamic loads.

Based on the target CoG and structural requirements, a preliminary electromechanical design for the ACCD is proposed. It includes the design of a diverging-converging RLV boom, which is received by a conical guiding cone at the ACCD's aft, and which is subsequently captured by an electromechanically actuated locking mechanism. A finite element analysis of this mechanism demonstrates the structural feasibility of this design, which achieves a safety factor of 1.55. Additionally, a study into the required performance of the locking actuators reveals that a combined docking-and-release mechanism is unfeasible, due to the presence of significant towing-induced friction at the contact interfaces. Instead, a separate release system is proposed, which relies on pyrotechnic fasteners to sever the towing connection between the TA and RLV.

To obtain size, weight, and power (SWaP) estimates for the ACCD's main avionics, commercial-off-the-shelf (COTS) solutions were used as a reference. Three operational modes were defined, from which overall power and energy requirements for the battery system were derived. These show that a system combining four 175 Wh lithium-ion batteries provides a 1.12 safety margin compared to the most conservative estimates. Additionally, the proposed mechanical integration of the battery system allows for scalability and modularity, tailored to the ACCD's energy needs.

Finally, an analysis of the ACCD's inertial properties was performed using a comprehensive computer-aided design (CAD) model. This results in a total functional mass estimate of 159.14 kg—representing a 28.4% increase compared to a reference mechanical design performed previously. Additionally, an analysis of the ACCD's CoG revealed the need for an additional 16.3 kg forward trim mass to meet the required target position. Compared to the reference design, this amounts to a 114% increase. Based on a breakdown of separate CoG contributions, the wings and guiding cone were observed to have the largest impact on the aft-located CoG. As such, future studies aiming to remove the need for a trim mass should reduce the mass of these assemblies first.

Going forward, it is highly recommended to perform physical prototyping of (parts of) the proposed ACCD design. This would generate invaluable insight into the behavior of this highly unique vehicle, while providing both quantitative and qualitative proof of its feasibility, reliability, and robustness. Based on experimental results for the relative navigation system, power system, docking mechanism, and overall towing system, conservative estimates and margins proposed in this work can then be relaxed. Conversely, it will also reveal where present analyses have not been conservative enough, and which subsystems need to be further improved. Doing so will greatly advance the technology readiness level of the ACCD in specific, and in-air capturing in general, supporting the push towards reusability across the European launcher industry.

Author Contributions B.L. developed the towing model, designed the docking mechanism, studied the avionics, and wrote the manuscript, S.S. supervised the study, provided reference data, and reviewed the manuscript, B.T.C.Z. supervised the study.

Funding Open Access funding enabled and organized by Projekt DEAL.

Data Availability No datasets were generated or analyzed during the current study.

Declarations

Conflict of interest The authors declare no conflict of interest.

References

1. Jenkins, D.R.: Space Shuttle: Developing an Icon—1972–2013. Specialty Press, (2017). ISBN: 978-1-58007-249-6
2. Stappert, S., Dietlein, I., Wilken, J., Bussler, L., Sippel, M.: Options for future european reusable booster stages: Evaluation and comparison of VTHL and VTVL return methods. CEAS Space J. **17**(1), 155–175 (2025). https://doi.org/10.1007/s12567-024-00571-x

3. Wilken, J., Herberhold, M., Sippel, M.: Options for future european reusable booster stages: evaluation and comparison of VTHL and VTVL costs. CEAS Space J. **17**(1), 177–198 (2025). https://doi.org/10.1007/s12567-024-00577-5
4. Schlögl, B.: Systematische analyse von ankopplungsverfahren zum bergen einer wiederverwendbaren raumtransporterstufe in der luft. DLR-Interner Bericht SART TN-008/2003, Köln, Germany (2003)
5. Singh, S., Mastrogiuseppe, M.: Multibody modelling of tether and capture system for dynamic simulations of In-Air-Capturing. Acta Astronaut. **218**, 59–69 (2024). https://doi.org/10.1016/j.actaastro.2024.02.008
6. Singh, S., Stappert, S., Bussler, L., Sippel, M., Kucukosman, Y.C., Buckingham, S.: Full-scale simulation and analysis of formation flight during In-Air-Capturing of a winged reusable launch vehicle. J. Space Safety Eng. **9**(4), 541–552 (2022). https://doi.org/10.1016/j.jsse.2022.09.005
7. Singh, S., Stappert, S., Buckingham, S., Lopes, S., Kucukosman, Y.C., Simioana, M., Pripasu, M., Wiegand, A., Sippel, M., Planquart P.: Dynamic modelling and control of an aerodynamically controlled capturing device for 'In-Air-Capturing' of a reusable launch vehicle. In: Proceedings of the 11th International ESA Conference on Guidance, Navigation & Control Systems (ESA GNC) (2021)
8. Singh, S., Luyten, B., Sagliano, M.: Relative navigation implementation for the in-air-capturing of a winged reusable launch vehicle. In: Proceedings of the 3rd International Conference on High-Speed Vehicle Science Technology (HiSST), Busan, South Korea (2024)
9. Kucukosman, Y.C., Lopes, S., Buckingham, S., Planquart, P., Singh, S., Bussler, L., Stappert, S., Sippel, M.: Aerodynamic characterization of In-Air Capturing vehicles using CFD simulations. In: Proceedings of the 9th European Conference for Aeronautics and Space Sciences (EUCASS), Lille, France (2022). https://doi.org/10.13009/EUCASS2022-7473
10. Stappert, S., Singh, S., Funke, A., Sippel, M.: Developing an innovative and high-performance method for recovering reusable launcher stages: the in-air capturing method. CEAS Space J. **16**, 411–426 (2023). https://doi.org/10.1007/s12567-023-00512-0
11. Singh, S., Sippel, M., Stappert, S.: Full-scale simulations of 'in-air capturing' return mode for winged reusable launch vehicles. J. Phys: Conf. Ser. **2526**, 012114 (2023). https://doi.org/10.1088/1742-6596/2526/1/012114
12. Briese, L.E., Gäßler, B.: Advanced modeling and trajectory optimization of the in-air-capturing maneuver for winged RLVs. Acta Astronaut. **193**, 756–766 (2022). https://doi.org/10.1016/j.actaastro.2021.09.005
13. Stappert, S.: Aerodynamics of the ACCD for the in-air-capturing of the SpaceLiner booster. DLR-Interner Bericht SART TN-016/2018, Bremen, Germany (2021)
14. Heide, J.: Auslegung eines kopplungsmechanismus für das in-air-capturing verfahren. DLR-Interner Bericht SART TN-004/2005, Köln, Germany (2005)
15. Atanassov, U.: Finite-elemente-analyse des 'in-air-capturing'-mechanismus mit dem programmsystem i-DEAS. DLR-Interner Bericht SART TN-005/2006, Köln, Germany (2006)
16. Kuk, T.: Active Control of Aerial Refueling Drogue. PhD thesis, Western Michigan University, Kalamazoo, United States of America (2014)
17. Choi, A.J., Park, J., Han, J.-H.: Automated aerial docking system using onboard vision-based deep learning. J. Aerosp. Inf. Syst. **19**(6), 421–436 (2022). https://doi.org/10.2514/1.I011053
18. Rodgers, L.P.: Concepts and Technology Development for the Autonomous Assembly and Reconfiguration of Modular Space Systems. Master's thesis, Massachusetts Institute of Technology, Boston, USA (2006)
19. Koziel, S., Pietrenko-Dabrowska, A.: Performance-Driven Surrogate Modeling of High-Frequency Structures. Springer Cham (2020). ISBN: 978-3-030-38926-0
20. Bussler, L.: Project FALCon: aerodynamic database of in-air-capturing candidate towing aircraft. DLR-Interner Bericht SART TN-012/2021 (2021)
21. Kucukosman, Y.C., Buckingham, S., Lopes, S., Planquart, P., Singh, S., Stappert, S., Bussler, L., Sippel, M.: CFD analysis of interaction effects between vehicles in formation flight for in-air capturing of reusable launchers. In: Proceedings of the 73rd International Astronautical Congress (IAC) (2022)
22. Luyten, B.: Icarus: In-Air Capturing Apparatus for Recovering Unpropelled Stages. Master's thesis, Delft University of Technology, Delft, The Netherlands (2024)
23. Singh, S., Bussler, L., Stappert, S., Sippel, M., Kucukosman, Y.C., Buckingham, S.: Simulation and analysis of pull-up manoeuvre during in-air capturing of a reusable launch vehicle. In: Proceedings of the 9th European Conference for Aeronautics and Space Sciences (EUCASS), Lille, France (2022)
24. National Oceanic and Atmospheric Administration. U.S. Standard Atmosphere, 1976. Technical Report NOAA-S/T 76-1562 (1976)
25. Singh, S., Bussler, L., Callsen, S., Stappert, S., Lopes, S., Buckingham, S.: A superposition approach to aerodynamic modelling of a capturing device used for in-air capturing of a reusable launch vehicle. In: Proceedings of the 9th European Conference for Aeronautics and Space Sciences (EUCASS), Lille, France (2022)
26. Singh, S., Bussler, L., Bergmann, K., Sippel, M.: Mission design and sensitivity analysis for in-air capturing of a winged reusable launch vehicle. In: Proceedings of the 74th International Astronautical Congress (IAC), Baku, Azerbaijan (2023)
27. Zipay, J.J., Modlin, C.T., Larsen, C.E.: The ultimate factor of safety for aircraft and spacecraft—its history, applications and misconceptions. In: Proceedings of the 57th AIAA/ASCE/AHS/ASC Structures, Structural Dynamics, and Materials Conference (SSDM) (2016). https://doi.org/10.2514/6.2016-1715
28. Sippel, M., Bussler, L., Krause, S., Cain, S., Stappert, S.: Bringing highly efficient RLV-return mode "in-air-capturing" to reality. In: Proceedings of the 1st International Conference on High-Speed Vehicle Science Technology (HiSST), Moscow, Russia (2018)
29. Barbetta, M., Boesso, A., Branz, F., Carron, A., Olivieri, L., Prendin, J., Rodeghiero, G., Sansone, F., Savioli, L., Spinello, F., Francesconi, A.: ARCADE-r2 experiment on board BEXUS 17 stratospheric balloon. CEAS Space J. **7**(3), 347–358 (2015). https://doi.org/10.1007/s12567-015-0083-3
30. Wittel, H., Jannasch, D., Vossiek, J., Spura, C. Roloff/Matek Machineonderdelen: Tabellenboek. Boom (2021). ISBN: 978-90-244-2868-7
31. Hatch, J.E.: Aluminum: Properties and Physical Metallurgy. American Society for Metals (1984). ISBN: 978-0-87170-176-3
32. Fritz Faulhaber GmbH & Co. Linear DC-servomotors with analog hall sensors. Technical report (2023)
33. Baumer. U300.D50-DPMJ.72N ultrasonic distance measuring sensor. Technical report (2024)
34. Omron Corporation. E3Z-G grooved-type photoelectric sensor with built-in amplifier. Technical report (2023)
35. Kwasi-Effah, C.C., Rabczuk, T.: Dimensional analysis and modelling of energy density of lithium-ion battery. J. Energy Storage **18**, 308–315 (2018). https://doi.org/10.1016/j.est.2018.05.002
36. Muralidharan, N., Self, E.C., Dixit, M., Zhijia, D., Essehli, R., Amin, R., Nanda, J., Belharouak, I.: Next-generation cobalt-free cathodes: a prospective solution to the battery industry's cobalt problem. Adv. Energy Mater. **12**(9), 2103050 (2022). https://doi.org/10.1002/aenm.202103050
37. Stenzel, P., Baumann, M., Fleer, J., Zimmermann, B., Weil, M.: Database development and evaluation for techno-economic assessments of electrochemical energy storage systems. In: Proceedings

of the 2014 IEEE International Energy Conference (ENERGYCON) (2014). https://doi.org/10.1109/ENERGYCON.2014.6850596

38. ACE Stoßdämpfer GmbH. ACE damping technology: Main catalogue 2017. Technical report (2017)